Dictyostelium chemotaxis

Kortholt, Arjan; Kataria, Rama; Keizer-Gunnink, Ineke; Van Egmond, Wouter N.; Khanna, Ankita; Van Haastert, Peter J. M.

Published in:
Embo Reports

DOI:
10.1038/embor.2011.210

Publication date:
2011

EMBO reports

scientific report

Dictyostelium chemotaxis: essential Ras activation and accessory signalling pathways for amplification

Arjan Kortholt, Rama Kataria, Ineke Keizer-Gunnink, Wouter N. Van Egmond, Ankita Khanna & Peter J.M. Van Haastert[+]

Department of Cell Biochemistry, University of Groningen, Groningen, The Netherlands

Central to chemotaxis is the molecular mechanism by which cells exhibit directed movement in shallow gradients of a chemoattractant. We used *Dictyostelium* mutants to investigate the minimal requirements for chemotaxis, and identified a basal signalling module providing activation of Ras at the leading edge, which is sufficient for chemotaxis. The signalling enzymes PI3K, TorC2, PLA2 and sGC are not required for Ras activation and chemotaxis to folate or to steep gradients of cAMP, but they provide a memory of direction and improved orientation of the cell, which together increase the sensitivity about 150-fold for chemotaxis in shallow cAMP gradients.

Keywords: chemotaxis; shallow gradients; Ras; amplification; synergy

EMBO *reports* (2011) **12**, 1273–1279. doi:10.1038/embor.2011.210

INTRODUCTION

An important aspect of cell motility is the ability of cells to respond to directional cues and display oriented migration (Van Haastert & Devreotes, 2004). Gradients of diffusive chemicals give rise to chemotaxis (Hoeller & Kay, 2007; Swaney *et al*, 2010). Chemotaxis has a pivotal role in finding nutrients in prokaryotes, forming multicellular structures in protozoa, tracking bacterial infections in neutrophils and organizing the embryonic cells in metazoa (Van Haastert & Devreotes, 2004). Sensitive cells, such as *Dictyostelium* or neutrophils, can detect very shallow spatial gradients of about 1% concentration difference across the cell (Mato *et al*, 1975).

The signal transduction cascade for chemotaxis consists of surface receptors, heterotrimeric and small G proteins, as well as several signalling enzymes, leading to the local activation of the cytoskeleton, predominantly F actin at the front and myosin filaments in the rear of the cell. In *Dictyostelium*, a shallow gradient of cyclic AMP induces the activation of cAMP receptors and their associated G proteins $G\alpha_2\beta\gamma$, in a manner that is approximately proportional to the steepness of the gradient (Xiao *et al*, 1997; Jin *et al*, 2000). In contrast, activation of Ras is much stronger in the front than in the rear of chemotaxing cells (Zhang *et al*, 2008). Four signalling enzymes, PI3K, TorC2, PLA2 and sGC, have been implicated in chemotaxis (Chen *et al*, 2007; Kamimura *et al*, 2008; Veltman *et al*, 2008; Liao *et al*, 2010). Activation of PI3K, TorC2 and sGC occurs downstream of Ras, and simultaneous disruption of both *rasC* and *rasG* results in the total loss of cAMP-mediated signalling (Bolourani *et al*, 2006; Kortholt & van Haastert, 2008).

A central question in chemotaxis is how these pathways allow efficient navigation of cells in very shallow gradients. Here we obtained quantitative data on Ras activation and chemotaxis in cAMP and folic acid gradients and report on the minimal requirements for chemotaxis of *Dictyostelium* cells.

RESULTS AND DISCUSSION

Ras activation is independent of the signalling pathways

Four signalling pathways, PI3K, TorC2, PLA2 and sGC, contribute to chemotaxis (Chen *et al*, 2007; van Haastert *et al*, 2007; Kamimura *et al*, 2008; Veltman *et al*, 2008). PI3K-mediated phosphorylation of Akt/PKB is completely inhibited by 20 μM LY, whereas TorC2-stimulated phosphorylation of PKBR1 is not inhibited by 20 μM LY but is strongly inhibited by 90 μM LY (Kamimura *et al*, 2008; Liao *et al*, 2010). Here we used *sgc/pla2*-null cells with 90 μM LY, by which all four pathways are inhibited. Similar results were obtained for two different cell lines in which all four signalling pathways are inhibited: *sgc/pla2/pkbR1*-null + 90 μM LY and *gc*-null + 90 μM LY + 2 μM BPB (inhibition of PLA2). To investigate the function of the signalling enzymes in directional movement, we obtained quantitative data on Ras activation and formation of F actin in the cortex, which can be detected as the translocation of Ras-binding domain (RBD)-Raf–GFP (green fluorescent protein) and LimEΔcoil–GFP, respectively.

Mutant cells with a deletion of the single *Dictyostelium gβ* gene do not show any chemotaxis, actin polymerization or Ras activation (data not shown (Wu *et al*, 1995; Sasaki *et al*, 2004)). Cells lacking either RasC or RasG exhibit good chemotaxis, whereas cells lacking both RasC and RasG move in random directions at all cAMP gradients tested (supplementary Fig S1A

Department of Cell Biochemistry, University of Groningen, Nijenborgh 7, 9747 AG Groningen, The Netherlands
[+]Corresponding author. Tel: +31 50 3634172; Fax: +31 50 3634165; E-mail p.j.m.van.haastert@rug.nl

Received 17 June 2011; revised 16 September 2011; accepted 22 September 2011; published online 11 November 2011

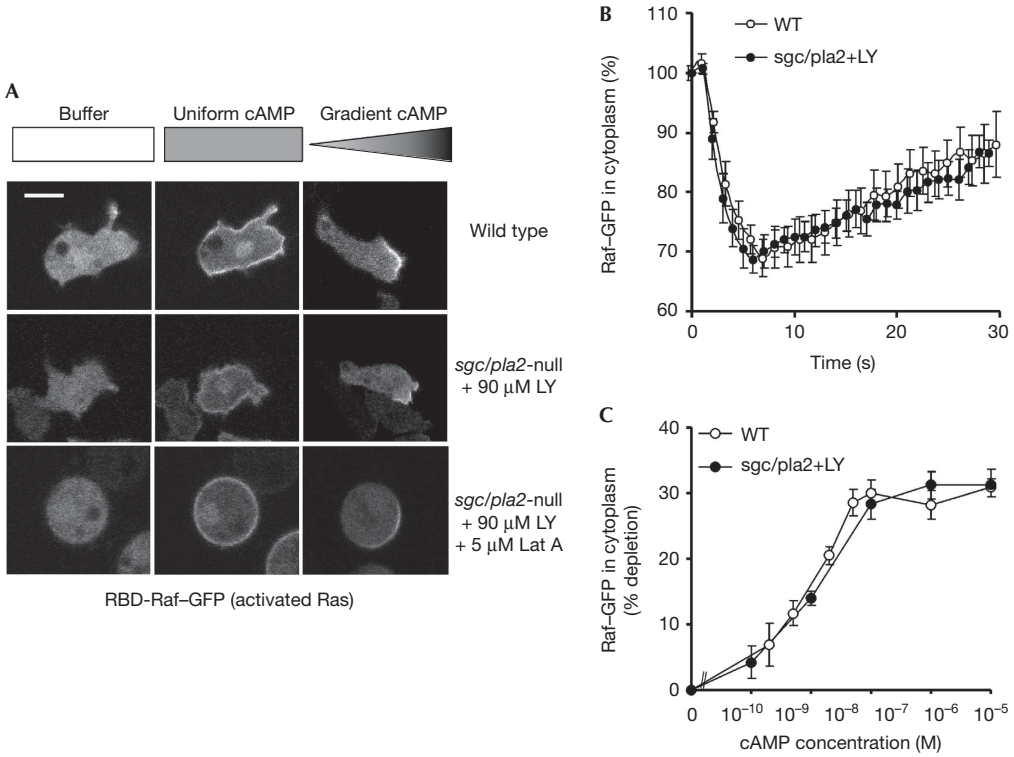

Fig 1 | Translocation of RBD-Raf–GFP from the cytoplasm to the cell boundary in wild-type cells, *sgc/pla2*-null cells with 90 μm LY and *sgc/pla2*-null/LY cells with 5 μM LatA. (**A**) Images of RBD-Raf–GFP-expressing cells in buffer, 3–6 s after the addition of uniform cAMP or in a cAMP gradient; scale bar, 5 μm. (**B**) The time course of translocation after uniform stimulation with 1 μM cAMP as means and s.e.m. of eight cells. (**C**) The response at 3–6 s after addition of uniform cAMP with different concentrations; shown are the means and s.e.m. of at least eight cells. cAMP, cyclic AMP; GFP, green fluorescent protein; LatA, Latrunculin A; WT, wild type.

online (Bolourani *et al*, 2006)). Furthermore, *rasC/G*-null cells do not exhibit RBD-Raf–GFP translocation to the membrane upon cAMP stimulation and have a very poor cAMP-stimulated F-actin response (supplementary Fig S1B online (Bolourani *et al*, 2006)). These experiments confirm that Gβγ and RasC/G are essential for chemotaxis (Wu *et al*, 1995; Sasaki *et al*, 2004). In wild-type cells, uniform cAMP induces a translocation of RBD-Raf–GFP and LimEΔcoil–GFP from the cytosol to the membrane (Fig 1; supplementary Fig S2 online). Mutant *sgc/pla2*-null/LY cells exhibit essentially the same response as wild-type cells (Fig 1; supplementary Fig S2 online). Furthermore, even *sgc/pla2*-null/LY cells incubated with 5 μM actin-polymerization inhibitor Latrunculin A show a Ras response that is indistinguishable from that of wild-type cells (Fig 1A).

Upon application of a cAMP gradient to wild-type cells, initially RBD-Raf–GFP transiently translocates uniformly to the cell boundary, which is then followed by RBD-Raf–GFP localization at the side of the cell facing the cAMP gradient (Fig 2A; supplementary Movie 1 online). Wild-type cells in a cAMP gradient are very polarized and exhibit strong localization of RBD-Raf–GFP in a well-defined crescent with a length of 4.4 ± 0.6 μm and an intensity that is 230 ± 50% above the intensity of the cytoplasm (mean and s.d., $n = 16$ cells, Fig 2A). In a steep cAMP gradient, mutant *sgc/pla2*-null/LY cells are less polarized and have a broader leading edge (Fig 2B); however, they show the accumulation of RBD-Raf–GFP and LimEΔcoil–GFP at the side of the cell facing the cAMP gradient, and cells exhibit significant chemotaxis (Figs 1,2; supplementary Fig S2 and Movie 2 online).

Consistent with a broader leading edge, RBD-Raf–GFP is enriched in a larger crescent with a length of 7.6 ± 0.6 μm and with a lower fluorescent intensity that is 130 ± 30% above the intensity of the cytoplasm. The amount of Ras activation, defined as the product of crescent size and increase of intensity, is not significantly different between wild-type (1,012 ± 260 μm%) and *sgc/pla2*-null/LY cells (988 ± 240 μm%). Wild-type cells treated with 5 μM Latrunculin A exhibit strong localized Ras activation in a cAMP gradient (Fig 1A; supplementary Movie 3 online). The length of the crescent is 7.5 ± 1.3 μm, with an intensity that is 155 ± 30% above the intensity of the cytoplasm (product 1,160 ± 300 μm%), similar to the crescent of *sgc/pla2*-null/LY cells. Together, these results show that Ras is activated at the leading edge through a pathway consisting of Gαβγ, which does not depend on the four signalling pathways or a functional cytoskeleton.

Chemotaxis in shallow cAMP gradients

The input signal for chemotaxis is a spatial gradient of cAMP, d*C*/d*x* (Mato *et al*, 1975). We measured Ras activation and chemotaxis of wild-type and mutant cells exposed to cAMP gradients with different steepness; see Postma and van Haastert (2009) for the equations that define the spatial gradient

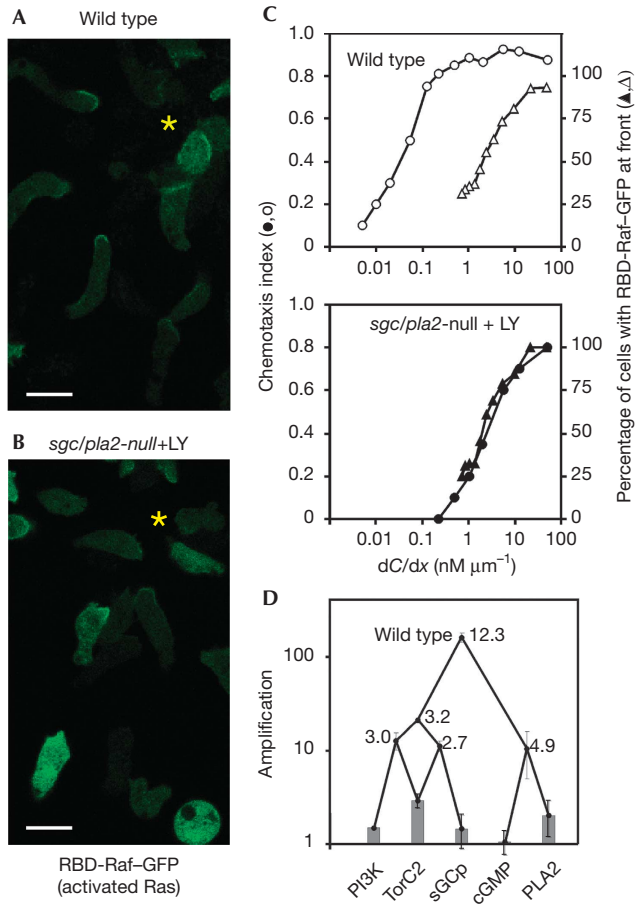

Fig 2 | Activation of Ras and chemotaxis in cAMP gradients. **(A,B)** Images from a movie of wild-type and *sgc/pla2*-null/LY cells, respectively. The asterisks indicate the position of the pipette; scale bar, 10 µm. The chemotaxis index and the fraction of cells with significant enhanced RBD-Raf–GFP at the leading edge were determined (defined as cells containing a fluorescence intensity of RBD-Raf–GFP at the leading edge that was at least 30% above the fluorescence intensity in the cytosol). **(C)** Strong Ras activation occurs only in steep gradients both in wild-type and *sgc/pla2*-null/LY cells. Chemotaxis of *sgc/pla2*-null/LY mutant cells occurs also only in these steep gradients, whereas wild-type cells exhibit chemotaxis in about 150-fold more shallow gradients. **(D)** A cluster analysis of amplification and synergy of signalling pathways derived from Table 1. The data points indicate the means and s.d. of amplification, and the numbers represent synergy (both obtained from Table 1). The tree was built by cluster analysis of the five pathways using the neighbour-joining method with synergy and amplification as distance measures. cAMP, cyclic AMP; GFP, green fluorescent protein.

at different distances from a pipette. Fig 2C presents the fraction of cells that exhibit significant enrichment of RBD-Raf–GFP at the leading edge (significant is defined as more than 30% above the intensity of the cytoplasm). These translocation experiments can only detect strong responses. Weak responses are undetectable, because boundary pixels are on average half filled with cytoplasm; as a result, the association of small amounts of RBD-Raf–GFP to the membrane does not result in a fluorescent intensity of the boundary pixel that is more than the fluorescent intensity in the adjacent cytosolic pixels (Bosgraaf *et al*, 2008). Half-maximal strong activation of Ras occurs at about 2,000 pM µm^{-1} in both wild-type and *sgc/pla2*-null/LY cells (Fig 2C). The data suggest that activation of Ras is essentially the same in wild-type and *sgc/pla2*-null/LY cells, except that in the mutant activation occurs in a broader leading edge. These results reveal that none of the four signalling enzymes (PI3K, TorC2, PLA2 and sGC), or potentially other enzymes inhibited by the high concentrations of LY294002, are involved in the transient activation of Ras to uniform cAMP, or persistent activation of Ras at the leading edge in a cAMP gradient.

Interestingly, chemotaxis of *sgc/pla2*-null/LY cells occurs in gradients with the same steepness as strong activation of Ras, whereas chemotaxis of wild-type cells is observed in spatial gradients that are about 150-fold smaller. Together, these experiments suggest that directional movement in the absence of the four pathways occurs without amplification of the spatial information that is carried by the localized Ras activation, whereas the four pathways allow chemotaxis to cAMP in very shallow gradients. During chemotaxis in natural cAMP waves, cells are exposed to cAMP gradients up to about 3,000 pM µm^{-1} (Tomchik & Devreotes, 1981; Postma & van Haastert, 2009). The results presented in Table 1 reveal that many mutants will chemotax in such gradients, despite their reduced sensitivity. This indicates that wild-type cells have a large spare sensitivity to tolerate non-optimal conditions in the soil; it also explains why many mutant cells show good cell aggregation under laboratory conditions.

Synergy provides amplification of cAMP gradient sensing

We determined the steepness of the cAMP gradient that induces half-maximal chemotaxis $(dC/dx)_{50}$ in a large collection of mutants (see supplementary Table S1 online). Wild-type cells exhibit half-maximal chemotaxis in a cAMP gradient of magnitude 22 pM µm^{-1}. Using three different cell lines in which all four pathways are inhibited, we obtained $(dC/dx)_{50} = 3{,}588 \pm 356$ pM µm^{-1}, which is about 150-fold larger than the $(dC/dx)_{50}$ of wild-type cells. To delineate the contribution of the pathways in amplification, we determined for many mutants the steepness of the gradient that induces half-maximal chemotaxis. In a mutant with pathway X active, the value of $(dC/dx)_{50}$ relative to 3,588 pM µm^{-1} of the four-pathway null mutant indicates the increase of sensitivity, or amplification, that is provided by pathway X.

When only one enzyme is active, chemotaxis occurs in slightly shallower gradients compared with the four-pathway null cells (Table 1). Expression of two pathways further increases sensitivity. Some combinations of pathways (for example, PI3K + sGC) exhibit a weak amplification, which in magnitude is similar to the product of the amplifications induced by the individual pathways, as would be expected for independent effects. However, other combinations (for example, PI3K + TorC2, sGC + TorC2 and sGC + PLA2) induce very good chemotaxis with strong amplification, indicating synergy of signalling pathways. The sGC enzyme has two functions in chemotaxis: one as a protein that localizes at the leading edge (sGCp), and one as enzyme producing cyclic GMP (cGMP; Veltman & van Haastert, 2006). By using two mutant proteins, namely sGCΔCat, which prevents cGMP synthesis, and sGCΔN, by which the protein becomes cytosolic but retains the ability to synthesize

Table 1 | Amplification of chemotaxis by synergy of signalling pathways

Active pathways	$(dC/dx)_{50}$ (pM μm^{-1})		Amplification		Synergy*
	Mean ± s.d.	N‡	Observed§	Expected‖	Mean ± s.d.
No active pathway	3,588 ± 356	7 (3), a	1.00		1.00 ± 0.10
PI3K	2,414 ± 89	3 (1), b	1.49		
TorC2	1,246 ± 218	6 (2), c	2.88		
PLA2	1,772 ± 375	3 (1), d	2.03		
sGC = (sGCp+cGMP)	1,848 ± 273	11 (4), e	1.94		
sGCp	2,474 ± 74	4 (1), f	1.45		
cGMP	3,417 ± 311	4 (1), g	1.05		
PI3K+TorC2	283 ± 60	6 (2), h	12.69	4.29	2.96 ± 0.82**
PI3K+PLA2	1,082 ± 225	3 (1), i	3.32	3.01	1.10 ± 0.33 NS
PI3K+sGC	1,025 ± 258	4 (2), j	3.50	2.89	1.21 ± 0.36 NS
TorC2+PLA2	430 ± 123	4 (1), k	8.34	5.83	1.43 ± 0.57 NS
TorC2+sGC	220 ± 20	14 (5), l	16.28	5.59	2.91 ± 0.71**
TorC2+sGCp	322 ± 12	4 (1), m	11.16	4.17	2.67 ± 0.48**
TorC2+cGMP	1,472 ± 69	4 (1), n	2.44	3.02	0.81 ± 0.16 NS
PLA2+sGC	296 ± 67	9 (4), o	12.11	3.93	3.08 ± 1.06**
PLA2+sGCp	975 ± 188	4 (1), p	3.68	2.94	1.25 ± 0.36 NS
PLA2+cGMP	343 ± 16	4 (1), q	10.47	2.13	4.92 ± 1.16**
PI3K+TorC2+PLA2	183 ± 27	4 (1), r	19.59	8.66	2.26 ± 0.71**
PI3K+PLA2+sGC	185 ± 14	4 (2), s	19.43	4.58	4.24 ± 1.05**
PI3K+TorC2+cGC	171 ± 9	6 (2), t	20.96	6.51	3.22 ± 0.67**
TorC2+PLA2+cGC	86 ± 12	9 (3), u	41.63	8.88	4.69 ± 1.51**
PI3K+TorC2+PLA2+sGC	22 ± 2	6 (1), v	162.69	13.19	12.33 ± 3.85**

Chemotaxis was tested to cAMP gradients with different steepness (as shown in Fig 2C). The spatial gradient that induces half-maximal chemotaxis is defined as $(dC/dx)_{50}$. Experiments were performed with various mutants and inhibitors to obtain cells with the combination of pathways active (see supplementary Table S1 online for these conditions). The s.d. for amplification and synergy were calculated using the mean and s.d. of the $(dC/dx)_{50}$ data; s.d. for amplification are not shown.
*Synergy is the observed amplification divided by the expected amplification. The significance of synergy was tested relative to 1.00 ± 0.10, the synergy for the condition 'no active pathway'; **$P<0.001$; NS, not significant at $P>0.05$. ‡Number of observations indicates total number of replicates with the number of strains in parenthesis. The letters refer to the strains used as indicated in supplementary Table S1 online. §Observed amplification: $(dC/dx)_{50}$ = 3,588 of 'no pathway' divided by $(dC/dx)_{50}$ of the specified active pathway. ‖Expected amplification is the product of observed amplifications of the individual pathways.
cAMP, cyclic AMP; PI3K, phosphoinositide kinase-3.

cGMP (Veltman & van Haastert, 2006), it could be shown that the cGMP function synergizes with PLA2, whereas the localization function of sGCp protein synergizes with TorC2 signalling (Table 1).

Cluster analysis was used to determine the interactions between signalling pathways for optimal synergy and amplification. The obtained tree presented in Fig 2D reveals two branches of synergizing activities, a branch with PI3K + TorC2 + sGCp, and a branch with cGMP + PLA2, respectively. Interestingly, this tree on chemotaxis has the same hierarchy as the tree that describes how signalling enzymes modulate pseudopodia in gradients of the chemoattractant (Bosgraaf & van Haastert, 2009; P.J.M. van Haastert, unpublished observations on TorC2 mutants). PI3K, sGCp and TorC2 are activated in the same region of the cell as activated Ras; that is, at the side of the cell facing the gradient (Funamoto *et al*, 2002; Veltman & van Haastert, 2006; Zhang *et al*, 2008), where they increase the probability that a pseudopod is formed. Thus, this synergizing cluster induces orientation of the cell towards the gradient. The second cluster consists of cytosolic cGMP and PLA2 (Chen *et al*, 2007), which are not involved in orientation but induce splitting of the current pseudopod (Bosgraaf & van Haastert, 2009). As a daughter-splitting pseudopod is extended in a similar direction to that of the parent pseudopod, the cGMP/PLA2 cluster functions as a memory of current direction.

In summary, one individual pathway does not contribute strongly to chemotaxis, but it can synergize with other pathways, which together increases the sensitivity about 150-fold.

Folate chemotaxis is independent of the pathways

Folate activates many signalling pathways in a way that is similar to activation by cAMP. Folate activates a folate receptor

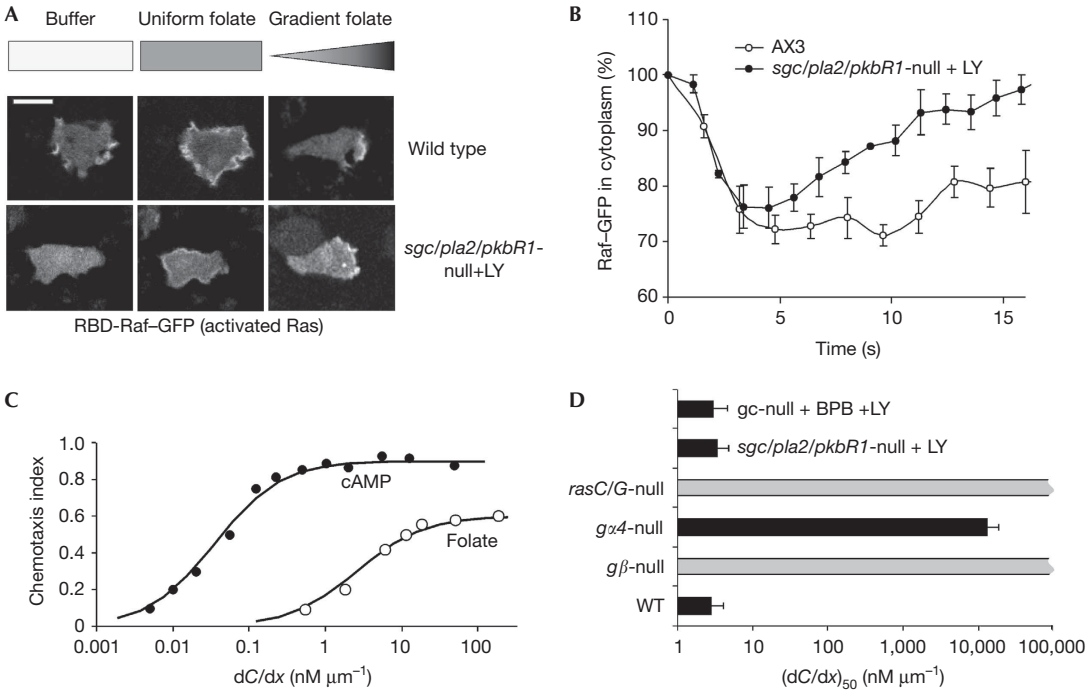

Fig 3 | Folate chemotaxis. (**A**) Images of RBD-Raf–GFP-expressing cells in buffer, 3–6 s after the addition of folate or in a folate gradient; scale bar, 5 μm. (**B**) The time course of translocation after uniform stimulation with 1 μM folate as means and s.e.m. of minimal seven cells. (**C**) The chemotaxis index of wild-type cells exposed to different spatial gradients of cAMP or folate. (**D**) The gradient inducing half-maximal folate chemotaxis $(dC/dx)_{50}$ was determined for the mutants shown; mutants *rasC/G*-null and *gβ*-null do not exhibit chemotaxis in the steepest gradient tested. The data shown are the means and s.d. of at least three experiments with at least 12 cells in each. Data for cAMP and folate chemotaxis were determined in cells starved for 5 and 0.5 h, respectively. cAMP, cyclic AMP; GFP, green fluorescent protein.

(De Wit & Bulgakov, 1985), predominantly the G protein $G\alpha_4\beta\gamma$ (Hadwiger *et al*, 1994), Ras (Lim *et al*, 2005) and the signalling enzymes PI3K, mTOR and guanylyl cyclase (Mato *et al*, 1977), leading to the formation of F actin and myosin filaments in the cortex (McRobbie & Newell, 1985). In a gradient of folate, Ras is activated at the leading edge with similar kinetics to that observed for cAMP (Fig 3A,B). The onset and magnitude of the response upon uniform stimulation are similar in wild-type and mutant cells lacking the four signalling enzymes, but recover faster in mutant cells (Fig 3A,B). Compared with cAMP chemotaxis, the response to folate requires steeper gradients, and the maximal chemotaxis index is smaller (Fig 3C; about 0.9 for cAMP versus about 0.6 for folate; the half-maximal response is about 0.3, and the gradient that induces a half-maximal response is defined as $(dC/dx)_{50}$). For wild-type cells, we observed half-maximal chemotaxis to folate with a gradient of $(dC/dx)_{50} = 2.8 \pm 1.4\ \text{nM}\ \mu\text{m}^{-1}$ (Fig 3D). Unexpectedly, inhibition of all four signalling enzymes had no effect on folate chemotaxis (Fig 3D). Mutant *sgc/pla2/pkbR1*-null cells in the presence of 20 μM LY or *gc*-null cells in the presence of BPB and LY exhibit chemotaxis in folate gradients that is at least as great as that of wild-type cells in the absence or presence of 20 μM LY. Although these pathways are activated well by uniform folate, and probably at the leading edge in a folate gradient (Mato *et al*, 1977; McRobbie & Newell, 1985; Lim *et al*, 2005; Liao *et al*, 2010), apparently this activity does not support chemotaxis. Possibly, the target enzymes are not activated strongly in vegetative cells.

Model for chemotaxis

Fig 4 combines previous and current experiments to yield a model for chemotaxis. Our results show that activation of Ras by cAMP is independent of the four signalling enzymes sGC, PLA2, PI3K and TorC2 and actin formation. Furthermore, none of the pathways are essential for chemotaxis to folate or to steep gradients of cAMP. As chemotaxis is completely lost in cells lacking Gβ (Wu *et al*, 1995) or RasC/G (Bolourani *et al*, 2006), we suggest a basal signalling module consisting of heterotrimeric and monomeric G proteins. This basal module provides activation of Ras at the leading edge, which is sufficient for chemotaxis. The next challenge will be to identify further components of this basal pathway and to determine the mechanism by which heterotrimeric G proteins induce Ras activation. As activation of Ras results in rapid actin polymerization, the basal module most probably will contain regulators of the cytoskeleton such as Rho family GTPases, ARP 2/3, WASP WAVE/Scar and mDIA (Stradal *et al*, 2004). The second module consists of the Ras-activated enzymes that induce amplification of gradient sensing. Activation of these enzymes at the leading edge has little effect on folate chemotaxis and is also not strictly essential for cAMP chemotaxis, but is very important to allow chemotaxis in shallow cAMP gradients. Important, but only partly known, are the interaction of these pathways with the cytoskeleton and the machinery of pseudopod formation. Positive and negative feedback loops between the different components in these two modules probably

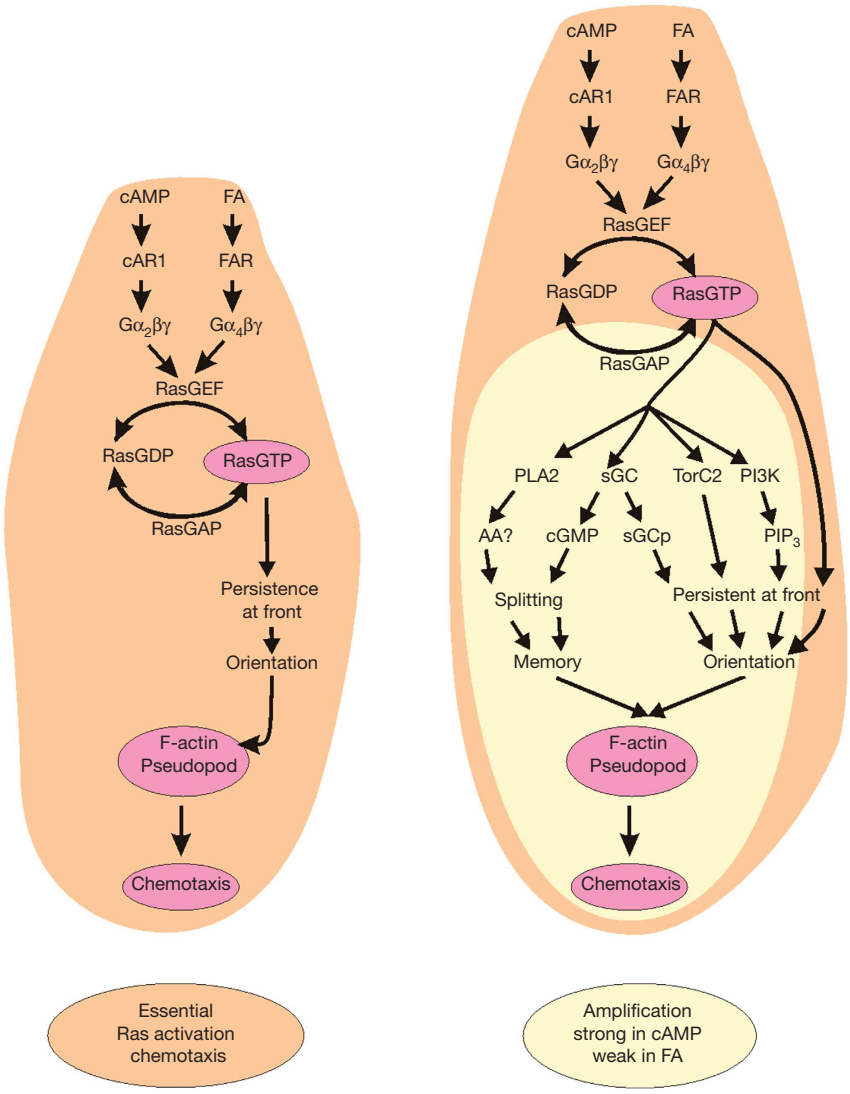

Fig 4 | Model for chemotaxis. A basal essential module provides prolonged activation of Ras and F actin at the leading edge of the cell, thereby inducing chemotaxis. This response occurs only in steep gradients. Amplification: activated Ras induces the activation of four signalling pathways. Strong synergy of PI3K, TorC2 and sGC protein at the leading edge induces the upgradient orientation of the cell. Synergy of cGMP and PLA2 induces splitting of the pseudopod, and as a daughter-splitting pseudopod is extended in a similar direction to that of the parent pseudopod, the cGMP/PLA2 cluster functions as a memory of current direction. Together, memory and orientation allow chemotaxis in more shallow cAMP gradients but have little effect on folate chemotaxis. AA, arachidonic acid; cAMP, cyclic AMP; FA, folic acid; FAR, folic acid receptor; PI3K, phosphoinositide kinase-3; PIP, phosphoinositides; PLA2, phospholipase A2; sGC, soluble guanylyl cyclase.

further enhance chemotaxis in shallow gradients. Therefore, this model provides a conceptual framework that can be used to identify critical components and missing links in chemotaxis, which might be useful to fine-tune and deepen our understanding of chemotaxis.

METHODS

Cell culture and preparation. The strains and conditions used in the chemotaxis experiments are described in supplementary Table S1 online (these strains have been described; see Veltman *et al*, 2008). The *sgc/pla2/pkbR1*-null strain was obtained by the inactivation of the *pkbR1* gene in *sgc/pla2*-null cells.

Cells were transformed with the plasmid pDm115RafRBD expressing RBD-Raf–GFP (amino acids 50–134 of RAF1) that binds to the activated GTP-bound state of Ras proteins (Kortholt & van Haastert, 2008), or plasmid LB15B expressing LimEΔcoil–GFP (amino acids 1–145 of LimE) that binds to F actin. Cells were grown in HL5-C medium including glucose (ForMedium), containing 50 μg ml^{-1}HygromycinB (Invitrogen) for selection. Cells were collected and suspended in 10 mM KH_2PO_4/Na_2HPO_4, pH 6.5 (phosphate buffer (PB)).

Chemotaxis assays. Chemotaxis was measured with the small population assay as described (Konijn, 1970), and with micropipettes (supplementary Table S1 online). To obtain mutant cells

that were in an optimal state for chemotaxis towards cAMP in the micropipette assays, unlabelled wild-type cells were mixed with equal amounts of green fluorescent protein (GFP)-tagged mutant cells and starved as a confluent layer (about 10^6 cells per cm^2) on plastic support for 5–7 h until streams started to form. Cells were collected in PB and incubated on a glass support at a lower density of approximately 4×10^4 cells per cm^2. The distance between adjacent cells is about 5 cell lengths, where cells do not form streams, and chemotaxis can be measured in the absence of strong interactions between mutant and wild-type cells. Chemotaxis was observed using a confocal fluorescent microscope, detecting wild-type and mutant cells in the phase-contrast and fluorescent channels, respectively.

For chemotaxis to cAMP, we used pipettes with a tip opening of 0.5 μm, containing 0.1 mM cAMP and operated at 0 or 25 hPa. For folate chemotaxis, the conditions were 1 μM or 1 mM folate, a pipette tip opening of 3 μm and a pressure of 1, 4 or 16 hPa. The actual gradient was measured with the fluorescent dye alexa 594 that was added to the chemoattractant solution, and the local concentration was recorded in the red channel of the confocal microscope (Postma & van Haastert, 2009). Most chemotaxis data were recorded at a distance x of 30–100 μm from the pipette. It holds that the concentration is given by $C(x) = xdC/dx$ (Postma & van Haastert, 2009).

Confocal images were recorded using a Zeiss LSM 510 META-NLO confocal laser scanning microscope equipped with a Zeiss plan-apochromatic $\times 63$ numerical aperture 1.4 objective. The chemotaxis index and speed were determined as described (Veltman & van Haastert, 2006). The fluorescent intensity of RBD-Raf–GFP in the cytoplasm was determined in large area selections of the cytoplasm using ImageJ. The crescent of RBD-Raf–GFP at the leading edge is defined as the area with fluorescent intensity that is at least 1.3-fold the fluorescent intensity of the cytoplasm. The fluorescent intensity of RBD-Raf–GFP in the crescent was determined with curved lines using ImageJ; the length of the crescent is defined as the length of the curved line. **Supplementary information** is available at EMBO *reports* online (http://www.emboreports.org).

ACKNOWLEDGEMENTS

We thank P. Devreotes, R. Firtel and the *Dictyostelium* stock center for providing *Dictyostelium* mutants. We thank D. Veltman for initial experiments on the F-actin response of *sgc/pla2*-null cells.

CONFLICT OF INTEREST

The authors declare that they have no conflict of interest.

REFERENCES

Bolourani P, Spiegelman GB, Weeks G (2006) Delineation of the roles played by RasG and RasC in cAMP-dependent signal transduction during the early development of *Dictyostelium discoideum*. *Mol Biol Cell* **17:** 4543–4550

Bosgraaf L, Keizer-Gunnink I, van Haastert PJ (2008) PI3-kinase signaling contributes to orientation in shallow gradients and enhances speed in steep chemoattractant gradients. *J Cell Sci* **121:** 3589–3597

Bosgraaf L, van Haastert PJ (2009) Navigation of chemotactic cells by parallel signaling to pseudopod persistence and orientation. *PLoS ONE* **4:** e6842

Chen L, Iijima M, Tang M, Landree MA, Huang YE, Xiong Y, Iglesias PA, Devreotes PN (2007) PLA_2 and PI3K/PTEN pathways act in parallel to mediate chemotaxis. *Dev Cell* **12:** 603–614

De Wit RJ, Bulgakov R (1985) Guanine nucleotides modulate the ligand binding properties of cell surface folate receptors in *Dictyostelium discoideum*. *FEBS Lett* **179:** 257–261

Funamoto S, Meili R, Lee S, Parry L, Firtel RA (2002) Spatial and temporal regulation of 3-phosphoinositides by PI 3-kinase and PTEN mediates chemotaxis. *Cell* **109:** 611–623

Hadwiger JA, Lee S, Firtel RA (1994) The G_α subunit $G_\alpha 4$ couples to pterin receptors and identifies a signaling pathway that is essential for multicellular development in *Dictyostelium*. *Proc Natl Acad Sci USA* **91:** 10566–10570

Hoeller O, Kay RR (2007) Chemotaxis in the absence of PIP3 gradients. *Curr Biol* **17:** 813–817

Jin T, Zhang N, Long Y, Parent CA, Devreotes PN (2000) Localization of the G protein βγ complex in living cells during chemotaxis. *Science* **287:** 1034–1036

Kamimura Y, Xiong Y, Iglesias PA, Hoeller O, Bolourani P, Devreotes PN (2008) PIP3-independent activation of TorC2 and PKB at the cell's leading edge mediates chemotaxis. *Curr Biol* **18:** 1034–1043

Konijn TM (1970) Microbiological assay of cyclic 3′,5′-AMP. *Experientia* **26:** 367–369

Kortholt A, van Haastert PJ (2008) Highlighting the role of Ras and Rap during *Dictyostelium* chemotaxis. *Cell Signal* **20:** 1415–1422

Liao XH, Buggey J, Kimmel AR (2010) Chemotactic activation of *Dictyostelium* AGC-family kinases AKT and PKBR1 requires separate but coordinated functions of PDK1 and TORC2. *J Cell Sci* **123:** 983–992

Lim CJ, Zawadzki KA, Khosla M, Secko DM, Spiegelman GB, Weeks G (2005) Loss of the *Dictyostelium* RasC protein alters vegetative cell size, motility and endocytosis. *Exp Cell Res* **306:** 47–55

Mato JM, Losada A, Nanjundiah V, Konijn TM (1975) Signal input for a chemotactic response in the cellular slime mold *Dictyostelium discoideum*. *Proc Natl Acad Sci USA* **72:** 4991–4993

Mato JM, van Haastert PJ, Krens FA, Rhijnsburger EH, Dobbe FC, Konijn TM (1977) Cyclic AMP and folic acid mediated cyclic GMP accumulation in *Dictyostelium discoideum*. *FEBS Lett* **79:** 331–336

McRobbie SJ, Newell PC (1985) Effects of cytochalasin B on cell movements and chemoattractant-elicited actin changes of *Dictyostelium*. *Exp Cell Res* **160:** 275–286

Postma M, van Haastert PJ (2009) Mathematics of experimentally generated chemoattractant gradients. *Methods Mol Biol* **571:** 473–488

Sasaki AT, Chun C, Takeda K, Firtel RA (2004) Localized Ras signaling at the leading edge regulates PI3K, cell polarity, and directional cell movement. *J Cell Biol* **167:** 505–518

Stradal TEB, Rottner K, Disanza A, Confalonieri S, Innocenti M, Scita G (2004) Regulation of actin dynamics by WASP and WAVE family proteins. *Trends Cell Biol* **14:** 303–311

Swaney KF, Huang CH, Devreotes PN (2010) Eukaryotic chemotaxis: a network of signaling pathways controls motility, directional sensing, and polarity. *Annu Rev Biophys* **39:** 265–289

Tomchik KJ, Devreotes PN (1981) Adenosine 3′,5′-monophosphate waves in *Dictyostelium discoideum*: a demonstration by isotope dilution–fluorography. *Science* **212:** 443–446

van Haastert PJ, Keizer-Gunnink I, Kortholt A (2007) Essential role of PI3-kinase and phospholipase A2 in *Dictyostelium discoideum* chemotaxis. *J Cell Biol* **177:** 809–816

Van Haastert PJM, Devreotes PN (2004) Chemotaxis: signalling the way forward. *Nat Rev Mol Cell Biol* **5:** 626–634

Veltman DM, Keizer-Gunnik I, van Haastert PJ (2008) Four key signaling pathways mediating chemotaxis in *Dictyostelium discoideum*. *J Cell Biol* **180:** 747–753

Veltman DM, van Haastert PJ (2006) Guanylyl cyclase protein and cGMP product independently control front and back of chemotaxing *Dictyostelium* cells. *Mol Biol Cell* **17:** 3921–3929

Wu LJ, Valkema R, Vanhaastert PJM, Devreotes PN (1995) The G-protein β-subunit is essential for multiple responses to chemoattractants in *Dictyostelium*. *J Cell Biol* **129:** 1667–1675

Xiao Z, Zhang N, Murphy DB, Devreotes PN (1997) Dynamic distribution of chemoattractant receptors in living cells during chemotaxis and persistent stimulation. *J Cell Biol* **139:** 365–374

Zhang S, Charest PG, Firtel RA (2008) Spatiotemporal regulation of Ras activity provides directional sensing. *Curr Biol* **18:** 1587–1593